

# Discovery potential of R-hadrons with the ATLAS detector

A. C. Kraan<sup>a,c</sup>, J.B. Hansen<sup>a</sup>, P. Nevski<sup>b</sup>

<sup>a</sup> *University of Copenhagen, Niels Bohr Institute, Blegdamsvej 17,  
2100 Copenhagen, Denmark*

<sup>b</sup> *Brookhaven National Laboratory, PO box 5000, Upton, NY., USA*

<sup>c</sup> *Current address: University of Pennsylvania, High Energy Physics,  
Department of Physics and Astronomy, 209 S. 33rd Street,  
Philadelphia, PA., USA*

## Abstract

The production of exotic heavy hadronic particles arise in several models for physics beyond the Standard Model. A study of the detection possibilities of new heavy hadron states with the ATLAS detector is presented. The focus is on R-hadrons, which are stable hadronized gluinos, predicted by certain supersymmetric models. Interactions and signatures of single R-hadrons are studied with the ATLAS simulation and reconstruction framework and issues concerning triggering on R-hadron events are addressed. The ATLAS fast simulation framework has been extended to include parameterizations for R-hadrons. Based on topological and kinematic variables only, the discovery potential of the ATLAS detector for R-hadron events produced in  $pp \rightarrow gg$  is studied for masses below  $2 \text{ TeV}/c^2$ . R-hadrons with masses as predicted by standard SUSY scenarios would be discovered already in the very early stages of the running of the LHC. The discovery reach of heavy gluinos, predicted by for example split supersymmetry models, extends up to at least  $1.8 \text{ TeV}/c^2$  for three years running of the LHC at low luminosity.

## 1 Introduction

Heavy stable hadrons are predicted in several extensions of physics beyond the Standard Model. For example, supersymmetry models exist in which the gluino is stable. Models with a gluino as lightest supersymmetric particle (LSP) are reviewed in Ref. [1], and include gauge mediated supersymmetry breaking models and string motivated supersymmetric models. Recently, stable gluinos with masses of the order of the TeV scale are predicted in the context of split supersymmetry models [2, 3]. A stable gluino would hadronize into heavy (charged and neutral) bound states. These bound states (for example  $\tilde{g}g$ ,  $\tilde{g}q\bar{q}$ ,  $\tilde{g}qqq$ ,  $\tilde{q}\bar{q}$ ,  $\tilde{q}qq$ ) are generically called R-hadrons, where the “R” refers to the fact that they can only be stable hadrons if R-parity is conserved [4]. Several models exist for the description of the interactions of stable hadrons in matter [1, 9]. The phenomenology of stable gluinos has been studied previously in Refs. [1, 5, 6, 7, 8, 9]. This paper discusses the discovery potential based on experimental studies of R-hadrons in the ATLAS detector at the LHC accelerator.

In addition to supersymmetry, other extensions of the Standard Model have been proposed, which predict the existence of new heavy stable hadrons, either due to the presence of a new conserved quantum number, or because the decays are suppressed by kinematics or couplings. Examples are theories with leptoquarks [10], theories with universal extra dimensions [11], theories with new Standard Model fermions [12] and certain unification models [13].

Various searches for stable massive particles have been performed. A comprehensive summary may be found in Refs. [14, 15]. The negative results of cosmic ray searches and searches in matter on earth suggests that these particles would not be strictly stable, so that all cosmological bounds can be evaded. In this note, a particle is referred to as stable as long as it does not decay in the detector. The mass range from accelerator searches is limited to the center of mass energy. In view of the existing mass limits, this study focuses on particles with masses  $\gtrsim 100 \text{ GeV}/c^2$ .

The detection of heavy non-hadronically interacting charged particles with the ATLAS detector has earlier been discussed in Refs. [16, 17]. In this paper, an extensive overview is presented on the interaction and detection of *hadronically interacting particles* in the ATLAS detector, with the focus on R-hadrons. Following the interaction model as proposed in Ref. [9], we discuss issues related to triggering, and study R-hadron signatures in the inner detector, calorimeters and muon chambers based on full simulation. Furthermore the discovery potential of the ATLAS detector with the LHC running at low luminosity ( $10 \text{ fb}^{-1}/\text{year}$ ) is investigated for gluinos with masses up to  $2 \text{ TeV}/c^2$ . More details about the simulation and analysis of R-hadrons can be found in Ref. [18].

The organization of this note is as follows. The production of R-hadrons at the LHC is described in Section 2. Section 3 summarizes the event generation for R-hadron and background events. The R-hadron event selection and resulting mass limit are discussed in Section 4. This section also includes a study of the most important signatures in the ATLAS detector as well as a discussion on trigger issues. In Section 5 several possible improvements are described which could extend the discovery reach of the ATLAS detector. Finally a summary is presented in Section 6.

## 2 R-hadron production

Gluino production is a purely strong process and depends, besides the gluino and squark masses, only on the strong coupling constant. A large number of gluinos (roughly  $10^8$  for

$m_{\tilde{g}}=100 \text{ GeV}/c^2$ ,  $10^3$  for  $m_{\tilde{g}}=1 \text{ TeV}/c^2$ ) is expected in one year of LHC running at low luminosity ( $10 \text{ fb}^{-1}/\text{year}$ ).

## 2.1 Production channels

At the LHC, gluinos will be produced via one of the processes  $\text{pp} \rightarrow \tilde{g}\tilde{g}$ ,  $\text{pp} \rightarrow \tilde{q}\tilde{q} \rightarrow \tilde{g}\tilde{g}q\bar{q}$ , or  $\text{pp} \rightarrow \tilde{q}\tilde{q} \rightarrow \tilde{g}\tilde{g}qq$ , where the latter two channels are only accessible if the squark is not too heavy. For  $\tilde{g}\tilde{g}$  production, the leading channels are  $q\bar{q} \rightarrow \tilde{g}\tilde{g}$  and  $gg \rightarrow \tilde{g}\tilde{g}$ . In this study, we focus on the channel  $gg \rightarrow \tilde{g}\tilde{g}$ , because this process is purely strong and, given the incoming beams and energies, depends only the gluino mass and the strong coupling constant. For moderate  $m_{\tilde{g}}$  (up to  $\sim 1400 \text{ GeV}/c^2$ ) this channel is dominating when considering  $\text{pp} \rightarrow \tilde{g}\tilde{g}$ . The ratio of the contribution to  $\tilde{g}\tilde{g}$  production from  $q\bar{q}$  to that of  $gg$  at the LHC is shown in Fig. 1a as function of  $m_{\tilde{g}}$  and  $m_{\tilde{q}}$ .

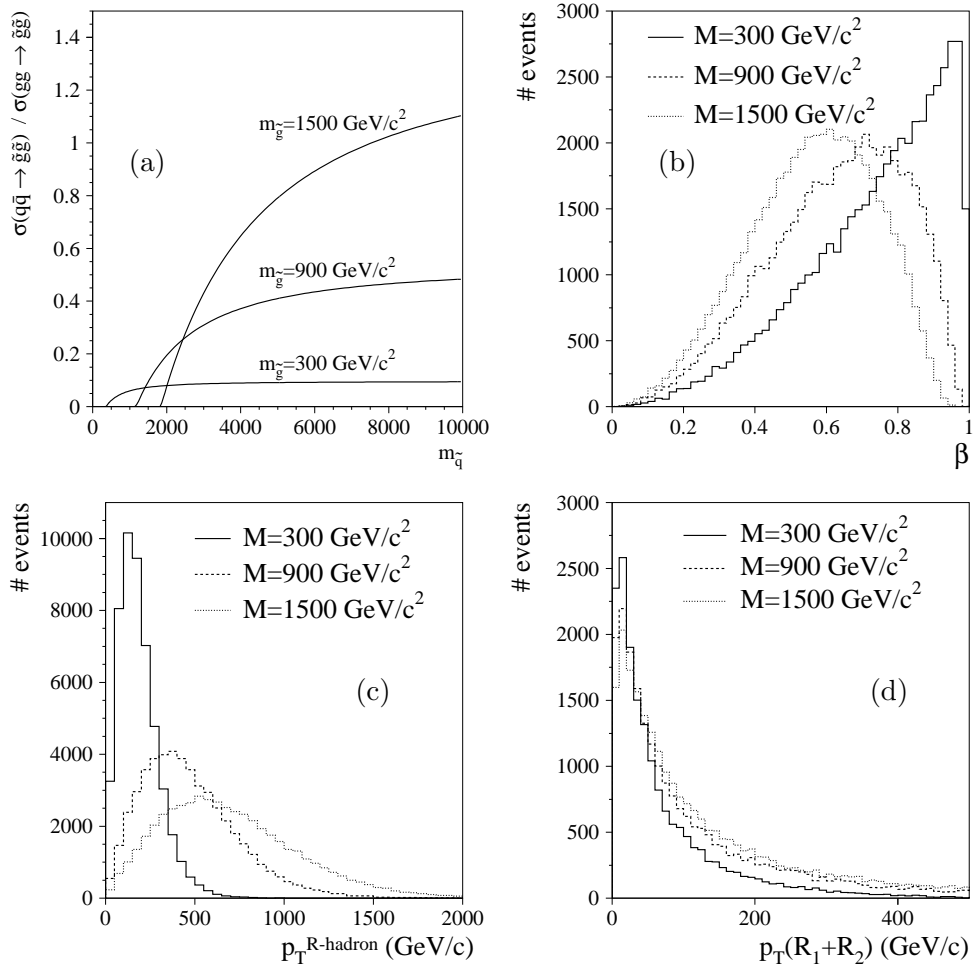


Figure 1: Aspects of R-hadron production. (a) The ratio of the contribution from  $q\bar{q}$  to that of  $gg$  at the LHC as function of  $m_{\tilde{g}}$  and  $m_{\tilde{q}}$ . (b) The distribution of the velocity of the R-hadrons produced at the LHC for  $m_{\tilde{g}}= 300, 900, 1500 \text{ GeV}/c^2$ . Average values are 0.74, 0.64 and 0.56 (c) The distribution of the transverse momentum of the R-hadrons produced at the LHC for  $m_{\tilde{g}}= 300, 900, 1500 \text{ GeV}/c^2$ , with average values 188, 427 and 699  $\text{GeV}/c$ . (d) The vector sum of the transverse momenta of the two R-hadrons, with average values of 74, 129 and 172  $\text{GeV}/c$ . For the distributions in (b), (c) and (d) only R-hadrons with  $|\eta| < 2.5$  were selected.

## 2.2 Gluino fragmentation

Long-lived gluinos hadronize into color singlet bound states. In the hadronization process, charged and neutral R-hadrons are produced ( $\tilde{g}q\bar{q}$ ,  $\tilde{g}qq\bar{q}$ ,  $\tilde{g}g$ ). For the detection of R-hadrons, it is crucial to know which hadron state is the lightest, since that state would dominantly be present in the detector (if it is indeed significantly lighter than the other states). The detection of neutral hadrons differs significantly from that of charged hadrons. The lightest hadron states turn out to be the R-mesons [9, 19, 20, 21], which are shown to be nearly mass degenerate, and slightly lighter than gluino-gluon states. R-baryons are also expected to be degenerate [9, 20], and are roughly  $0.3 \text{ GeV}/c^2$  heavier than the R-mesons. Thus, there is no preference for an R-hadron to be charged or neutral. The probability to form a  $\tilde{g}g$  bound state is a free parameter, taken to be 0.1 by default [22]. No  $\tilde{g}\tilde{g}$  -states are considered in the present study and thus R-hadrons are always produced in pairs. For the remaining fraction, the probability to form a neutral and charged R-hadron is about half-half. Only a small amount of baryons ( $\sim 2\%$ ) are formed due to baryon suppression. In the present study, gluino hadronization is performed using dedicated PYTHIA routines [22].

## 2.3 Event topology

The combination of phase space, matrix elements and parton density functions results in heavy particles being produced at a  $p - p$  collider like the LHC with high  $p_T$  values, typically of the order of their own mass, i.e. they may be relativistic but their mass is still far from negligible. The R-hadrons produced in the channel  $pp \rightarrow \tilde{g}\tilde{g}$  events are characterized by two R-hadrons produced approximately in a back-to-back configuration in the transverse plane. The likely presence of a missing energy signal depends among others on the R-hadron mass, because heavier R-hadrons are generally produced with higher momenta than lighter R-hadrons, and thus may result possibly in a larger imbalance. The distribution of the velocity and transverse momentum of the R-hadrons produced at the LHC via  $gg \rightarrow \tilde{g}\tilde{g}$  is shown in Fig. 1b and c for different masses of the gluino. Figure 1d shows the total transverse momentum of the two R-hadrons produced via  $gg \rightarrow \tilde{g}\tilde{g}$ .

### 2.3.1 Isolation

Since we expect muons to be the dominant background source, the jet structure around the gluino is investigated at event generator level and compared to that of isolated muons and non-isolated muons produced via b-quark decay. For this study, 50000  $pp \rightarrow Z/\gamma \rightarrow \mu^+\mu^-$  events and 50000  $pp \rightarrow Z/\gamma \rightarrow b\bar{b}$  events, with  $b$  decaying weakly into muons, have been generated, and compared to R-hadrons of mass  $300 \text{ GeV}/c^2$ , produced via  $pp \rightarrow \tilde{g}\tilde{g}$  and  $pp \rightarrow \tilde{q}\tilde{q} \rightarrow \tilde{g}\tilde{g}qq$ . In all cases the  $\hat{p}_T$  of the hard  $2 \rightarrow 2$  process was required to be more than  $50 \text{ GeV}/c$ . Figure 2 shows the distribution of the number of particles, the particles density, and the total  $p_T$  of the particles in a cone of size  $R = \sqrt{\Delta\eta^2 + \Delta\phi^2}$  around the muon or R-hadron, excluding the muon or R-hadron itself (and neutrinos).

## 3 Event simulation

### 3.1 R-hadron event simulation

There are no models available which propose definite gluino LSP masses following from GUT scale assumptions. Thus, the gluino LSP mass at the electroweak scale is a free parameter.

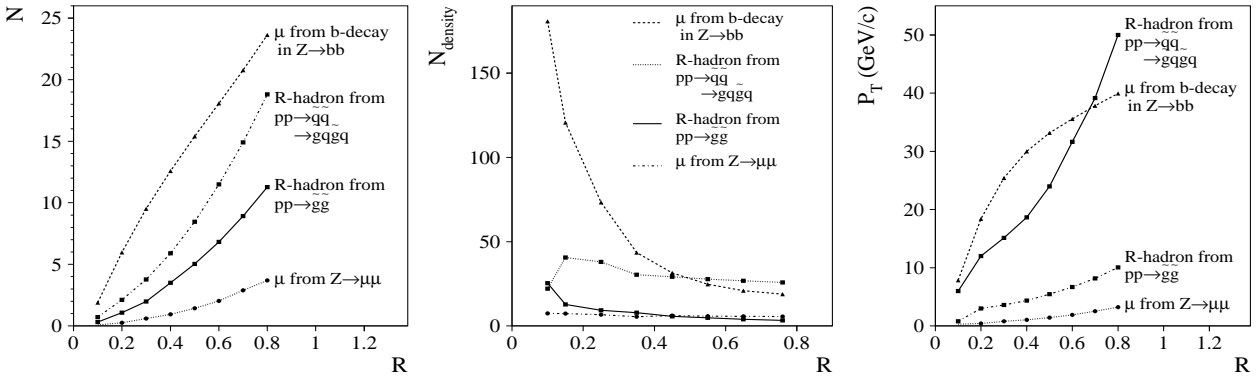


Figure 2: A comparison of the jet structure between muons from  $pp \rightarrow Z/\gamma \rightarrow \mu^+\mu^-$ , muons from  $pp \rightarrow Z/\gamma \rightarrow b\bar{b}$ , and 300  $\text{GeV}/c^2$  R-hadrons produced via  $pp \rightarrow \tilde{g}\tilde{g}$  and  $pp \rightarrow \tilde{q}\tilde{q} \rightarrow \tilde{g}\tilde{g}qq$ . The mass of the squark was 800  $\text{GeV}/c^2$  [23]. Left: mean value of the average number of particles  $N$  in a cone around the muon direction as function of the cone radius  $R$ . Middle: mean value of the particle density  $N_{\text{density}}$  around the muon direction as function of the cone radius  $R$ . Right: mean value of the transverse momentum,  $p_T$ , in a cone around the muon or R-hadron direction as function of the cone radius  $R$ .

Below we concentrate entirely on the channel  $gg \rightarrow \tilde{g}\tilde{g}$ . Since the cross section for this channel depends only on the gluino mass, none of the masses of the other supersymmetric particles is relevant, as long as they are heavier than the gluino to assure non-decaying gluinos. The gluino masses investigated are  $m_{\tilde{g}} = 100, 300, 600, 900, 1100, 1300, 1500, 1700$  and  $1900 \text{ GeV}/c^2$  and events were generated with PYTHIA [22].

The ATLAS fast simulation framework is used to simulate R-hadrons in the detector and perform the physics analysis. The framework is extended to account for R-hadrons, using parameterizations of the momentum resolution of inner detector, the response in the calorimeter, and the response in the muon spectrometer. The parameterizations come from studying signatures in the different ATLAS sub-detectors for singly charged R-mesons of various masses ( $100 \text{ GeV}/c^2$  to  $1900 \text{ GeV}/c^2$ ), transverse momenta and pseudo-rapidity ( $\eta$ ). These have been fully simulated using the ATLAS detector simulation framework based on GEANT3 [24], and subsequently reconstructed with the ATLAS C++ reconstruction framework. A detailed discussion of the GEANT3 [24] implementation of the model used can be found in Refs. [9, 18]. For the resolution of the inner detector momentum, the parameterization followed quite well that of muons in ATLAS [25], after an additional contribution due to multiple scattering (proportional to  $1/(\beta p)$ ), especially important for slow R-hadrons, was included.

Typically, the momentum resolution,  $\sigma(1/p_T)$ , is of the order of 0.005. Details on the response of the calorimeters and the muon chambers, forming the base for the parameterizations, are described in Section 4.1. Further information on the parameterizations can be found in Ref. [18].

### 3.2 Background simulation

QCD processes with their high cross section present a potential background problem for studies of hadronic particles. Fortunately, the cross section for QCD events drops rapidly with increasing transverse momentum scale in the hard process ( $\hat{p}_T$ ), and the  $p_T$  of the hadronized particles is further suppressed by the soft fragmentation function of light partons. Moreover, the long lifetime of pions and kaons effectively prevents them from decaying into muons before they get

absorbed in the calorimeter. However, the weak decays of high  $p_T$  b-quarks and t-quarks will produce high  $p_T$  muons, and thus present a serious background. For the QCD background, separate samples have been generated for light quarks (denoted by QCD), b-quarks (denoted by  $b\bar{b}$ ), and t-quarks (denoted by  $t\bar{t}$ ). QCD  $b\bar{b}$  and  $t\bar{t}$  events have been generated in logarithmic  $\hat{p}_T$  bins. The number of generated events in each  $\hat{p}_T$  bin is assured to be larger than that corresponding to  $1 \text{ fb}^{-1}$ . The only exception to this rule is in the region of very small  $\hat{p}_T$ , which have very large cross sections, but out of several millions of generated events, no events pass the trigger cuts. Generating a number of events corresponding to  $1 \text{ fb}^{-1}$  is beyond the scope of this work, and would only be relevant for a QCD trigger rate study.

Also, events with single Z and W production as well as events where two gauge bosons (denoted by WW/WZ/ZZ) form a potential background source. Such events may result in muons, and these events are likely to pass the trigger criteria. The  $p_T$  value for most muons produced from Z and W is of the order of  $M_Z/2$ , and thus on average smaller than those of R-hadrons. Thus, we expect much of this background to be effectively removed by a  $p_T$  cut on muons. The generation of Z, W, and diboson events is also done in bins. The width of the bins is optimized according to the cross section, and the number of generated events in each  $\hat{p}_T$  bin is assured to be larger than that corresponding to  $1 \text{ fb}^{-1}$ .

## 4 Event selection

Due to their slow movement, yet high momentum, and their composite colored structure, with one constituent being ultra heavy, R-hadrons posses very distinct features when they traverse ordinary matter. The typical signatures for the detection of single heavy stable hadrons are

- High transverse momentum for charged hadrons.
- Large ionization in the tracking system, in case the R-hadrons are charged and slow.
- A characteristic pattern of energy deposition in the calorimeters.
- A large time-of-flight, measurable with the muon chambers.

### 4.1 R-hadron triggers

Prior to selection, events are required to pass a set of trigger requirements. With their special signatures, R-hadrons may fall outside the standard trigger categories available in ATLAS [26, 27]. In the following we discuss the most relevant criteria for R-hadron events. The ATLAS triggers studied in this paper are given in Table 1. The studied triggers can be classified in two groups: calorimeter triggers and muon triggers. For the former, it is hard to estimate the efficiency precisely, because it depends on the details of the trigger reconstruction algorithms. The muon triggers turn out to be the most promising.

#### 4.1.1 Calorimeter triggers

Two aspects must be kept in mind when studying the interactions of R-hadrons in the calorimeter. First of all, an R-hadron passing the ATLAS calorimeters will undergo repeated charge flipping in subsequent interactions ( $\sim 12$ ) through the calorimeter. Hence, the results presented here are independent of the initial charge of the R-hadron for the momentum range studied. Second, an R-meson will convert to an R-baryon due to repeated nuclear interactions, because

Menu	Requirement
$1\mu 6$	One muon, which has $p_T > 6 \text{ GeV}/c$ <sup>1</sup> .
$2\mu 10$	Two muons, each of which has $p_T > 10 \text{ GeV}/c$ .
$1\mu 20i$	One isolated muon with $p_T > 20 \text{ GeV}/c$ .
$E_{T}^{miss} > 70 \text{ GeV}$	and a jet with $E_T > 70 \text{ GeV}$ .
$j400$	Jet $E_T > 400 \text{ GeV}$ .
$2j350$	Two jets, each of which has $E_T > 350 \text{ GeV}$ .
$E_{T}^{miss} > 200 \text{ GeV}$	

Table 1: Trigger menus, as defined in Ref. [27]. These trigger menus are still subject to changes.

this is kinematically favorable [9]. Once the R-hadron is baryon, the nuclear cross section is  $3/2$  larger [9] and thus energy losses due to nuclear scattering increase.

The energy deposit and the possible stopping of R-hadrons in the calorimeters depend on the number of interactions an R-hadron undergoes when passing the calorimeters and the actual energy loss per interaction. In Fig. 3a, the number of interactions for an R-hadron traversing the ATLAS calorimeters is displayed as a function of  $\eta$ . The typical energy loss per interaction in iron for an R-hadron with a mass of  $300 \text{ GeV}/c^2$  is shown in Fig. 3b. As can be seen from this plot, the energy loss for an R-hadron tends to level off for very high energies. For an R-hadron which punches through the calorimeter and passes the support structure to arrive at the first muon-station the number of interactions is about 15% higher.

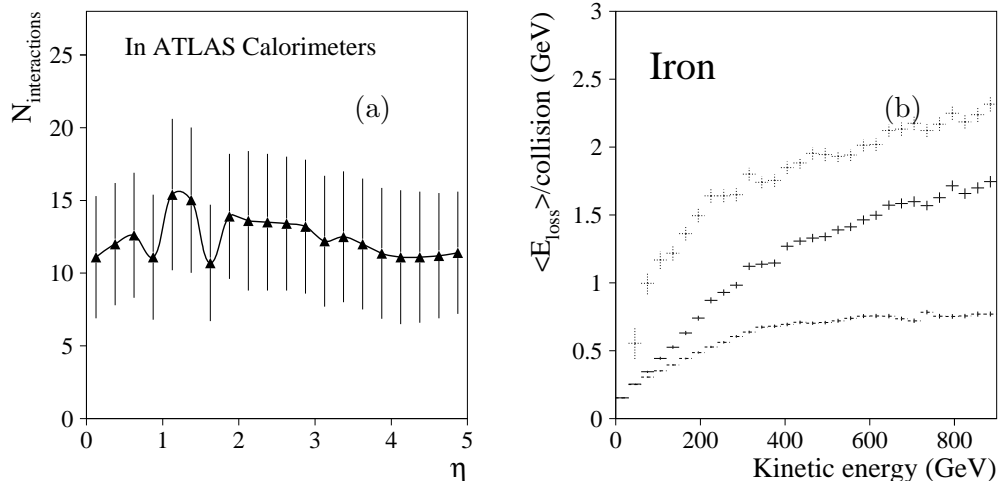


Figure 3: (a) The average number of interactions and its spread at the exit of the ATLAS calorimeter system as function of  $\eta$ , for a R-hadron punching through the ATLAS calorimeters. These results are for full simulation with the ATLAS detector simulation framework based on GEANT3 and reconstruction with the ATLAS C++ reconstruction framework. (b) The average energy loss per interaction in iron for an R-hadron with a mass of  $300 \text{ GeV}/c^2$ . The lower and upper curves correspond to the energy loss enabling only  $2 \rightarrow 2$  and  $2 \rightarrow 3$  scattering, respectively, and the middle histogram represent the combination [9].

The total energy deposit measured in the ATLAS calorimeters is displayed as function of  $\eta$  for various R-hadrons masses and transverse momenta in Fig. 4. This figure shows that the

<sup>1</sup>Introduced in Ref [26], but removed in Ref [27] due to the higher (doubled) expected initial luminosity at the LHC startup. The local threshold for *individual* muons in the ATLAS muon-system is still  $p_T > 6 \text{ GeV}/c$ .

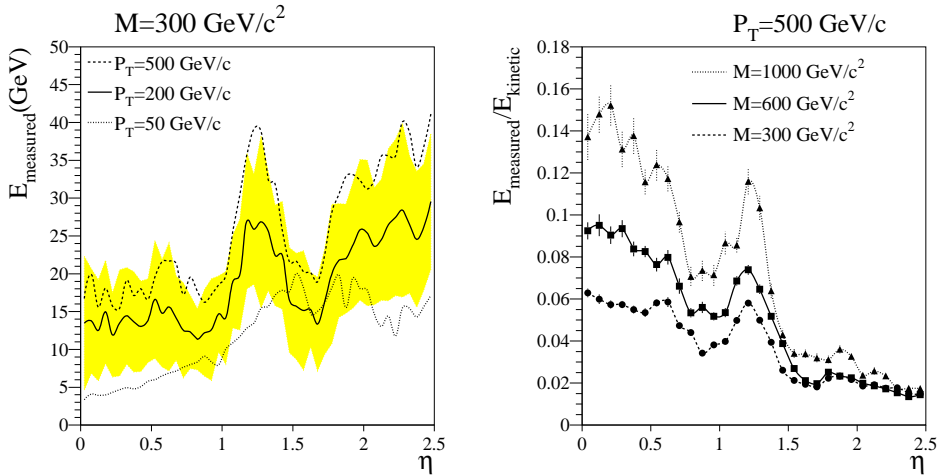


Figure 4: Energy loss for punch-through R-hadrons. On the left-hand side the absolute energy loss is shown as function of  $\eta$  for different transverse momenta. The shaded area represents the spread in the energy deposit for R-hadrons with mass  $300 \text{ GeV}/c^2$  and  $p_T$  of  $500 \text{ GeV}/c$ . On the right-hand side the relative energy deposition is plotted for R-hadron masses of  $300$ ,  $600$  and  $1000 \text{ GeV}/c^2$  with a transverse momentum of  $500 \text{ GeV}/c$ . Results are obtained by full simulation with the ATLAS detector simulation framework based on GEANT3 and reconstruction with the ATLAS C++ reconstruction framework.

relative energy loss drops with higher kinetic energy.

**Impact on Trigger** The first level trigger is based on a quick analysis of the regions of interest (ROI's) in the calorimeters and the muon system, while at higher level the information is combined with tracking information [27]. Thus, for R-hadrons, it is crucial to understand the interplay between the information accessible at the different trigger levels: for example, it could happen that one charged and one neutral R-hadron are produced. Depending on the details of the trigger algorithm (for example if it uses energy flow or not), and on whether a charged R-hadron reaches the muon chamber, this could result in a large  $E_T^{miss}$ . However, certainly no such imbalance is present if considering the calorimeters alone, and it is therefore possible that it does not pass the first level calorimeter trigger, only using calorimeter energy clusters. The same situation may happen for the jet-based triggers: an R-hadron energy deposit rarely will give rise to a very high energetic jet in the calorimeters by itself, but including the possible charged track information in the final event reconstruction will result in a high  $p_T$  jet.

An additional complication arises for the calorimeter triggers if the R-hadrons would be heavily delayed. In this case the R-hadron signal would perhaps not be suitable for the trigger electronics to reconstruct the full pulse-shape of the signal, resulting in a lower reconstructed energy. Fortunately this is expected to have a small effect for two reasons. Firstly, the delay in arrival at the calorimeters is typically small (distance less than 4m), such that it is possible to adjust the delay timing to account for this if necessary. Secondly, for triggers based on  $E_T^{miss}$  it must be noted that if an R-hadron energy deposit would not result in a ROI, this would result in an even higher missing energy signal.

In conclusion, an R-hadron event is most likely to pass the first level trigger when the energy deposit in the calorimeters results in an  $E_T^{sum}$  or  $E_T^{miss}$  trigger signal. Given the large transverse energy values required by the triggers defined in Table 1, only a small fraction of R-hadrons are expected to pass the first level calorimeter triggers. The corresponding high level triggers will be passed if the  $E_T^{sum}$  or  $E_T^{miss}$  are large, but the high level trigger includes the momentum

measurement of the inner detector and that of the muon chambers. Given the large momentum values of the R-hadron tracks, this will usually result in a trigger signal for either the  $E_T^{\text{sum}}$  or  $E_T^{\text{miss}}$  trigger – provided the first level trigger is passed, most likely with another trigger signature.

#### 4.1.2 The muon trigger

The possibility to use the muon trigger for the detection of slow charged particles, not interacting hadronically, has already been investigated for the central region of the ATLAS detector [16]. The trigger efficiencies were estimated by requiring a coincidence between the two involved trigger stations within a time window of 18 ns. For low luminosity, the efficiency of the trigger was found to be as high as 90% for slow particles with  $\beta = 0.2$ . However, such slow particles would arrive at the muon stations 125 ns after the bunch crossing, or 100 ns after an ordinary muon would arrive. Thus, when the muon trigger condition is met, and data-taking started, the information of an event which came four bunch crossings later is recorded, and the relevant information of the slow particle from the inner detector and calorimeters is probably already lost. To which extent the relevant information is available, depends on the velocity of the R-hadron and the detailed timing of the signal in the different subsystems.

For the following discussion, one should keep in mind that a priori only about 75% of all R-hadrons shows up as charged in the muon system irrespective of their original charge and type (R-meson or R-baryon) when they were formed. This is due to the many repeated nuclear interactions upstream to the muon system, after which an R-hadron independently of it being an R-meson or R-baryon will end up as either a charged (3 states) or neutral (1 state) R-baryon at the muon chambers. This effect is included in the estimates presented in Table 4.

**Estimate of muon trigger efficiency based on full simulation** The ATLAS muon trigger has 2 different configurations using different muon stations, depending on the instantaneous luminosity [25]. For low luminosity the trigger requires a coincidence between the two barrel RPC's (Resistive Plate Chambers) positioned at approximately 6.7 (1st RPC) and 7.5 m (2nd RPC) from the interaction point, or the two endcap TGC's (Thin Gas Chambers) located at approximately 14 (2nd TGC) and 14.5 m (last TGC). At high luminosity, a coincidence is required between different muon stations: the two barrel RPC's situated at approximately 6.7 (1st RPC) and 10 m (last RPC), or the two endcap TGC's placed at approximately 13 (1st TGC) and 14.5 m (last TGC). The efficiency of the muon trigger is studied by requiring in addition that the R-hadron is recorded in the correct event.

The conditions of an R-hadron firing the muon trigger and being assigned to the right event are then the following

- The R-hadron arriving at the muon stations must be charged and must have  $\eta < 2.5$ .
- The R-hadron has a coincidence in the two trigger stations within the temporal gate of the trigger stations, which is taken to be 18 ns [16] for both barrel and endcap trigger stations. For example, for the RPC's at  $\theta = 0^0$ , this would correspond to  $\beta > 0.5$  for the high luminosity trigger stations and  $\beta > 0.14$  for the low luminosity trigger stations.
- The delay of a heavy particle compared to that of a muon must be less than 25 ns, so that the trigger is fired within the right event. This puts an upper limit on the maximum

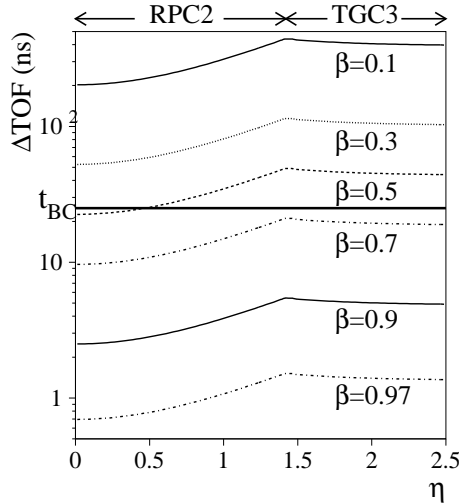


Figure 5: The difference in time-of-flight  $\Delta\text{TOF}$  at RPC2 (7.5 m) and TGC3 (14.5 m) between a non-interacting particle traveling with velocity  $\beta$  in a certain  $\eta$ -region, and a particle traveling with the speed of light, as function of  $\eta$ . The bunch crossing time  $t_{BC}$  is the maximum difference allowed by the trigger.

time-of-flight (TOF) of a particle at the trigger stations<sup>2</sup>. In Fig. 5, the difference in time-of-flight  $\Delta\text{TOF}$  between a non-interacting particle with  $\beta < 1$  and a particle with  $\beta = 1$  at RPC2 (7.5 m) and TGC3 (14.5 m) is shown. The latter stations are the last involved stations for a low luminosity muon trigger. Looking at the central detector region ( $\eta = 0$ ), we see that the particle must have  $\beta \gtrsim 0.5$  in order to reach the last trigger station (7.5 m) in time. For a high luminosity trigger making use of the last trigger station in the barrel region (10 m), this limit would be  $\beta > 0.6$ . In Fig. 6, the delay at the last trigger stations for low luminosity is shown for fully simulated R-hadrons of mass  $300 \text{ GeV}/c^2$  of different  $p_T$  values as function of  $\eta$ . Due to the increased energy loss per nuclear scattering, a light R-hadron is more delayed than a heavy one with the same starting velocity, when measured in the muon system, as shown in Fig. 8.

- The deflection angle of the R-hadron in the magnetic field must be smaller ( $p_T$  greater) than that of the corresponding muon (6 or  $10 \text{ GeV}/c$ ). Since R-hadrons are produced with high momenta, this condition is always satisfied.

The  $1\mu 6$  and the  $2\mu 10$  trigger menus have been simulated by requiring R-hadrons to satisfy the above criteria and the resulting trigger efficiencies are shown in Table 2 for  $\text{pp} \rightarrow \tilde{g}\tilde{g}$ .

In the calculations of the efficiencies of the muon trigger, all charged R-hadrons reaching the muon chambers are assumed to produce hits in *all* the trigger planes. Due to support structures and the presence of the magnet, it is possible that additional nuclear reactions may take place. For high  $p_T$  muons, the probability to undergo a nuclear interaction is very small, and the efficiency of a muon to fire the trigger is very close to 100% [25]. For an R-hadron, however, the probability for nuclear interactions is considerably larger. Since the support structures depend on  $\eta$ , the probability has been evaluated with full simulation in five different  $\eta$  regions. The results, shown in Table 3, show that there is indeed a non-zero probability that an R-hadron interacts in the muon system and possibly converts into another R-hadron with a different charge.

<sup>2</sup>The TOF information in GEANT is not available by default and has been introduced in the ATLAS detector simulation framework based on GEANT3 for this purpose.

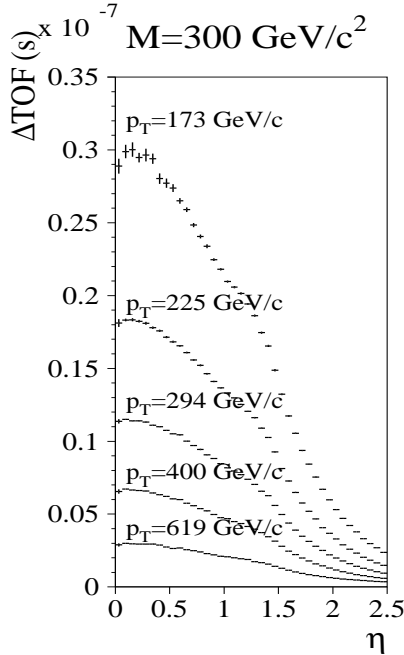


Figure 6: The difference in time of flight  $\Delta\text{TOF}$  as function of  $\eta$  at RPC2 and TGC3 between an R-hadron of mass  $300 \text{ GeV}/c^2$  and a particle traveling with  $\beta = 1$ . The displayed momenta correspond to  $\beta$ -values at  $\eta = 0$  of 0.5, 0.6, 0.7, 0.8, 0.9 and 0.98.

Trigger	Mass	Luminosity	Efficiency (%) $\text{pp} \rightarrow \tilde{g}\tilde{g}$
$1\mu 6^3$	100	Low	61
		High	58
	300	Low	67
		High	63
	600	Low	60
		High	59
$2\mu 10$	100	Low	28
		High	24
	300	Low	33
		High	29
	600	Low	34
		High	27

Table 2: An estimate of the trigger efficiency for  $\text{pp} \rightarrow \tilde{g}\tilde{g}$  events. These results are based on fully simulated charged R-mesons in the ATLAS detector and requiring the conditions given in Section 4.1.2.

This aspect introduces an important extra uncertainty for the muon triggers and tracking in the muon chambers.

**Effects of the time delays on the R-hadron measurement** Even if the R-hadron fires the muon trigger in time to be recorded within the right event, it is not a priori certain whether the detector information of all the separate subsystems can still be used when building the full

region	$\eta$	5-10 m (total)	6.7-7.5 m (LL)	6.7-9.9 m (HL)
barrel:	$\eta(0, 0.5)$	30%	7%	17%
	$\eta(0.5, 1.0)$	40%	10%	30%
	$\eta(1.0, 1.5)$	45%	7%	15%
region	$\eta$	7-15 m (total)	14.1-14.5 m (LL)	12.9-14.5 m (HL)
endcap	$\eta(1.5, 2.0)$	60%	2%	3%
	$\eta(2.0, 2.5)$	75%	2%	3%

Table 3: Fraction of R-hadrons undergoing one or more nuclear interactions in the muon system. The probabilities are displayed for the entire system, and for the region in between the two trigger stations at low (LL) and high (HL) luminosity.

event.

For the pixels and silicon detectors, the following can be remarked. First of all, the delay in the central region is very small (maximum 1 and 2 ns for pixels and silicon, respectively), since their location is very close to the vertex. Second, for these detectors a hit is based on detecting a certain amount of charge [28]. Slow R-hadrons are late, but would be heavily ionizing and certainly result in a hit. Third, we only make use of these detectors for momentum measurements, requiring only the hit positions, rather than the whole signal shape. Thus, the information of these subdetectors is reliable, if indeed we require the R-hadron to arrive at the muon chambers with a delay smaller than 25 ns.

For the TRT, the delay is slightly larger, maximally (for an R-hadron with velocity  $\beta = 0.5$ ) about 4 ns at the outer layers at 1.1 m. However, this delay is only a small fraction of the maximum drift time is of 40 ns, and it would correspond to a drift distance of only 200  $\mu\text{m}$ . A good reconstruction of the signal is probably possible.

For the calorimeters, the time-interval over which data taking stretches in case of a positive trigger signal is roughly 125 and 175 ns for LAr and Tile calorimeters, respectively. Thus the signal can probably be fully reconstructed, although the resolution may be worse due to the time-shift w.r.t. a standard signal, for which the detector readout and timing have been optimized.

#### 4.1.3 Trigger rates

The ATLAS trigger possibilities is estimated by making a pseudo-trigger, which includes the trigger menus as defined in Table 1. The pseudo-trigger distinguishes between a 'first level trigger', where only calorimeter information and the muon triggers are used, and a 'high level trigger', using all possible information.

The trigger simulation assumes the LHC to be running in the *low luminosity mode*, because the cross sections for gluino production are anyway high, and the low luminosity muon trigger has a larger efficiency than the high luminosity trigger.

In Table 4 the numbers of events expected in  $1 \text{ fb}^{-1}$  after triggering are summarized for different R-hadron masses and background processes.

<sup>3</sup>Due to the higher expected initial luminosity at the LHC startup, the  $1\mu 6$  trigger menu is no longer included, and is replaced by the  $1\mu 20$ . This has no impact on the R-hadron signal.

Sample	$N_{\text{trig}}(1 \text{ fb}^{-1})$
$M_R = 100$	$3.6 \times 10^7$
$M_R = 300$	$2.0 \times 10^5$
$M_R = 600$	$3.6 \times 10^3$
$M_R = 900$	$2.3 \times 10^2$
$M_R = 1100$	$4.9 \times 10^1$
$M_R = 1300$	$1.1 \times 10^1$
$M_R = 1500$	3.2
$M_R = 1700$	0.9
$M_R = 1900$	0.3
QCD	$6.5 \times 10^8$
$b\bar{b}$	$4.9 \times 10^8$
W	$1.1 \times 10^7$
Z	$5.3 \times 10^6$
diboson	$1.6 \times 10^5$

Table 4: The number of triggered events for R-hadrons of various masses and for the background sources for an integrated luminosity of  $1 \text{ fb}^{-1}$ .

## 4.2 R-hadron event selection

A schematic overview of the R-hadron overall behavior in the ATLAS detector is shown in Fig. 7.

In the following two selection approaches have been investigated. First, a selection is performed on the basis of *event topology* alone. This represents what can be done within the present analysis framework, i.e. standard event filter, and which does not require a very fine level of simulation of the response of the ATLAS detector. Second, another selection procedure is presented requiring a more detailed study of the possibilities to measure the R-hadron time-of-flight or velocity.

### 4.2.1 Event selection variables

Three variables related to the global event topology have been investigated:

**The transverse momentum in the muon chambers:** The transverse momentum of the most energetic muon or R-hadron in the muon chambers, denoted by  $P_T^{\mu,R}$ .

**The missing transverse energy,  $E_{\text{miss}}^T$ :** A vector sum of the transverse momenta of all particles, calculated using full event information, i.e. also taking into account the inner detector and the muon chambers. For charged R-hadrons detected in the inner detector, the  $p_T$  of the track is counted in the vector sum, while for neutral R-hadrons the transverse energy as measured in the calorimeter is counted. However if the R-hadron is detected in the muon chambers, but not in the inner detector, the  $p_T$  as measured in the muon chambers is counted. If it is detected in both, matching is assumed possible, and only the inner detector is counted in that case.

**The total visible energy of the event,  $E_{\text{sum}}^T$ :** A scalar sum over transverse energies of all particles, using the same event information content as  $E_{\text{miss}}^T$ .

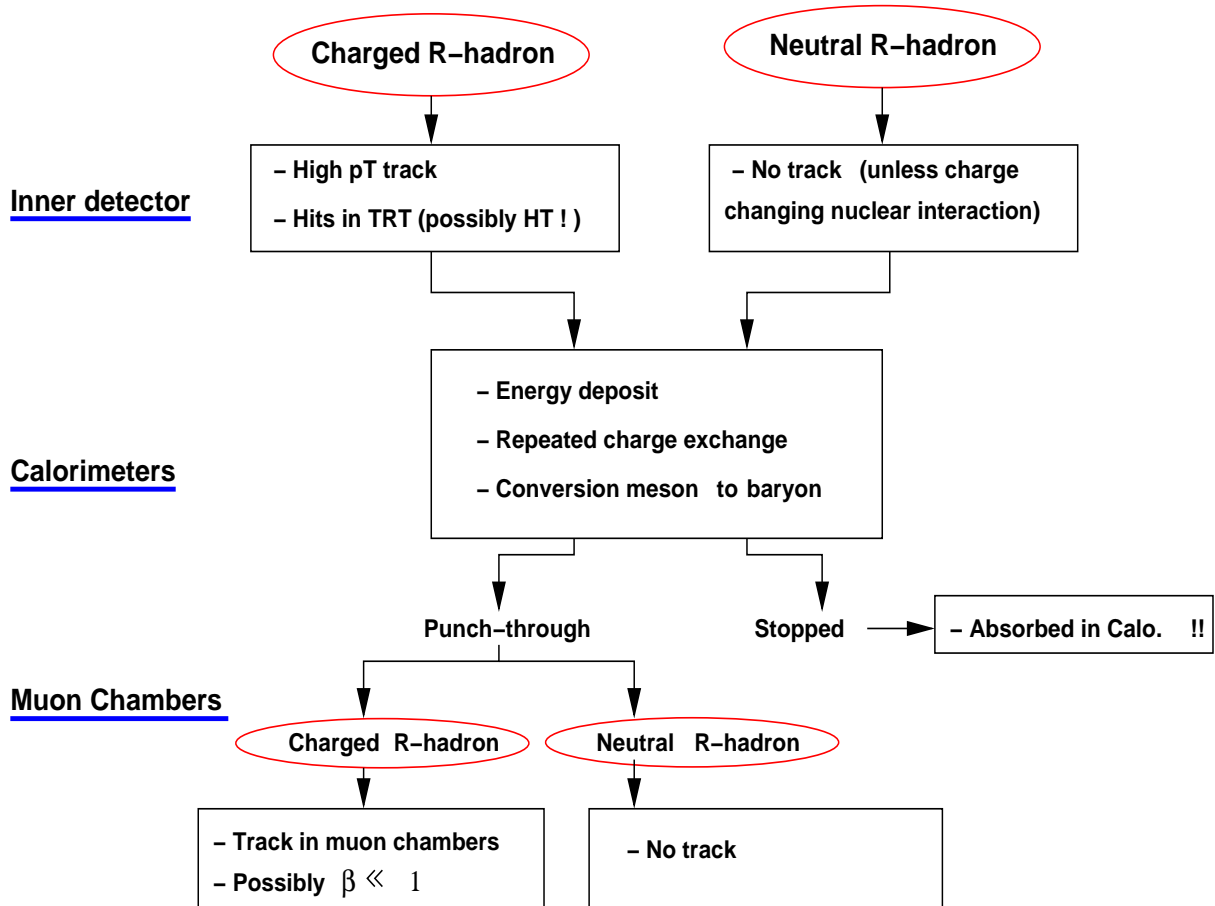


Figure 7: Possible manifestations of an R-hadron in ATLAS.

Distributions of the three variables for signal and background after high level trigger cuts are shown in Fig. 10. Figure 11 shows the  $E_{miss}^T$  distribution for R-hadron events where only calorimeter information is used (like the first level trigger), events where only the transverse momentum of one the two R-hadrons is measured, and events where two charged R-hadrons are measured. Note the significant difference in the average  $E_{miss}^T$ .

**Time-of-flight to the muon chambers.** The difference in time-of-flight to the muon chambers,  $\Delta\text{TOF}$ , between an R-hadron and a muon, is a more involved variable, requiring a modified track reconstruction in the muon chambers. An estimate of the accuracy of the ATLAS muon chambers to measure time-of-flight as well as velocity is given in the following.

Time-of-flight measurements in ATLAS are possible due to the staggered arrangement of the MDT's (Monitoring Drift Tubes) in the muon chambers and an excellent timing precision ( $\simeq 1$  ns) of the MDT's. From the tube staggering the  $\chi^2$  of the fitted trajectory is sensitive to the particle velocity, thus providing a tool to reconstruct  $\beta = v/c$  [17]. Following the method of Ref. [17], based on  $\chi^2$  minimization w.r.t.  $\beta$  of a track, the velocity of R-hadrons is determined using the muon system. The resulting resolution of the R-hadron velocity in the production vertex is found to be

$$\sigma(\beta)/\beta^2 = 0.067 \pm 0.029. \quad (1)$$

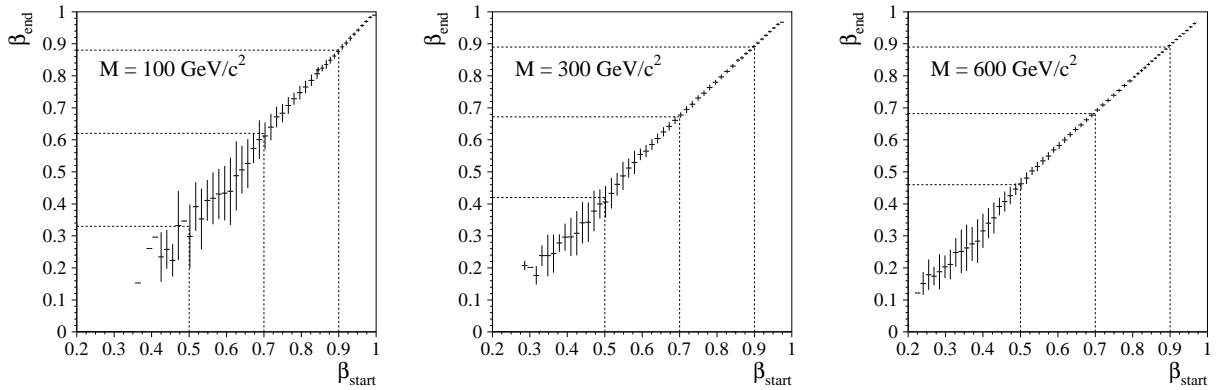


Figure 8: The velocity  $\beta_{end}$  as measured at the second layer of MDT's (7.11 m) in the central barrel region ( $\eta = 0.1$ ) as function of the velocity  $\beta_{start}$  at the vertex. The error bars correspond to the spread on the mean value.

It must be noted that R-hadron energy losses in the calorimeter result in a significantly smaller velocity at the muon chambers than that at the primary vertex. As a result of the fluctuations in energy loss, the error of the production velocity prediction is increased comparing to the velocity measured in the muon system itself.

In Fig. 8 the velocity of R-hadrons at the second (middle) layer of MDT's ( $r = 7.11$  m),  $\beta_{end}$ , is shown as function of the  $\beta_{start}$ , the velocity at the vertex. A distribution of the velocity at the muon chambers is shown in Fig. 9 for an R-hadron and a particle without hadronic losses. Thus, as a result of the fluctuations in energy loss for a hadronic particle, the error of the production velocity prediction is increased comparing to the velocity measured in the muon system itself.

The resolution of the velocity measurement by the muon chambers of R-hadrons given above is used to parameterize the transverse momentum measurements by the muon chambers (see first item). In the following, we also use the  $\simeq 1$  ns timing precision of the ATLAS muon system directly by cutting on the measured time-of-flight of R-hadrons compared to that of muons.

#### 4.2.2 Selection procedure

The definition of the signal significance,  $P$ , follows that of the ATLAS physics performance study [25],

$$P = \frac{S}{\sqrt{B}}, \quad (2)$$

where  $S$  and  $B$  are the number of background and signal events, respectively. The usual criterion for discovery is a signal significance greater than 5 and at least 10 observed signal events. Different cuts apply for different R-hadron mass samples. In Table 5, the cuts for all mass samples are summarized. The corresponding selected number of events for signal and background as well as the  $S/\sqrt{B}$  ratios are listed in Table 6.

These cuts are all related to the global shape and kinematics of the events, i.e. on information available at high level trigger.

Another selection procedure, requiring a more detailed knowledge of the detector and the event reconstruction as the method described above, would be to measure the velocity of the R-hadrons and muons using the muon chambers, and to extract the time-of-flight information. The intrinsic time resolution of the muon chambers is about 1 ns [17]. Requiring the  $\Delta$ TOF with

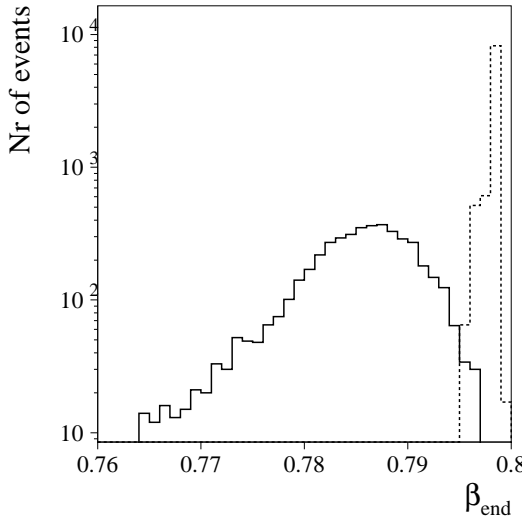


Figure 9: The distribution of  $\beta_{end}$  as measured at the first layer of MDT's (6.92 m) when  $\beta_{start} = 0.8$ , for a strongly interacting particle (solid), and for a particle only interacting electromagnetically (dashed), both of mass 300  $\text{GeV}/c^2$ . The spread in  $\beta_{end}$  is much larger for a strongly interacting particle, as expected.

respect to a particle with  $\beta = 1$  to be larger than 3 ns (conservatively  $\gtrsim 3\sigma$ ) yields a powerful rejection against muons. Thus, for this method the  $\Delta\text{TOF}$  replaces the cuts on missing energy and total transverse energy sum, while the cut on the muon transverse momentum is unchanged. For heavy R-hadrons (masses above 1  $\text{TeV}/c^2$ ) the  $\beta$  is typically 0.8 or smaller and a tighter cut on the time delay could be used, but the limiting factor for discovery is the gluino production cross-section. Table 7 shows the corresponding  $S/\sqrt{B}$  values.

### 4.3 Results and discussion

Using only global event variables, available from standard high level event reconstruction, R-hadrons can be discovered for masses up to 1400  $\text{GeV}/c^2$  for an integrated luminosity of 30  $\text{fb}^{-1}$  assuming low luminosity muon trigger configurations. In particular, for low masses, a signal significance of 5, the usual criterion for discovery, could be reached after only a few days of running. Including more specialized information from a dedicated reconstruction, such as time-of-flight, improves the sensitivity and pushes the discovery limit for R-hadron masses up to 1700  $\text{GeV}/c^2$ . The numbers in Table 5 represent conservative estimates, as we do not include the model-dependent contributions from  $q\bar{q} \rightarrow \tilde{g}\tilde{g}$ , which, for high gluino masses, can be larger than 100%, see Fig. 1a. For example, in the framework of split supersymmetry with very high squark masses, the discovery potential would extend up to masses of 1600  $\text{GeV}/c^2$  if only using global event shape variables, and up to 1800  $\text{GeV}/c^2$  if time-of-flight information would be included.

Although the high luminosity muon trigger configuration has not been studied, the reduction in muon trigger efficiency is small, as seen in Table 2. A reduction of less than 50  $\text{GeV}/c^2$  in discovery potential is expected.

There are a number of uncertainties that may influence the precise discovery limit for R-hadrons and in the following we discuss the most important sources.

The probability to obtain a gluino-gluon state in the hadronization process,  $P_{\tilde{g}g}$ , by default taken to be 0.1, is directly related to the ratio of charged to neutral R-mesons produced in

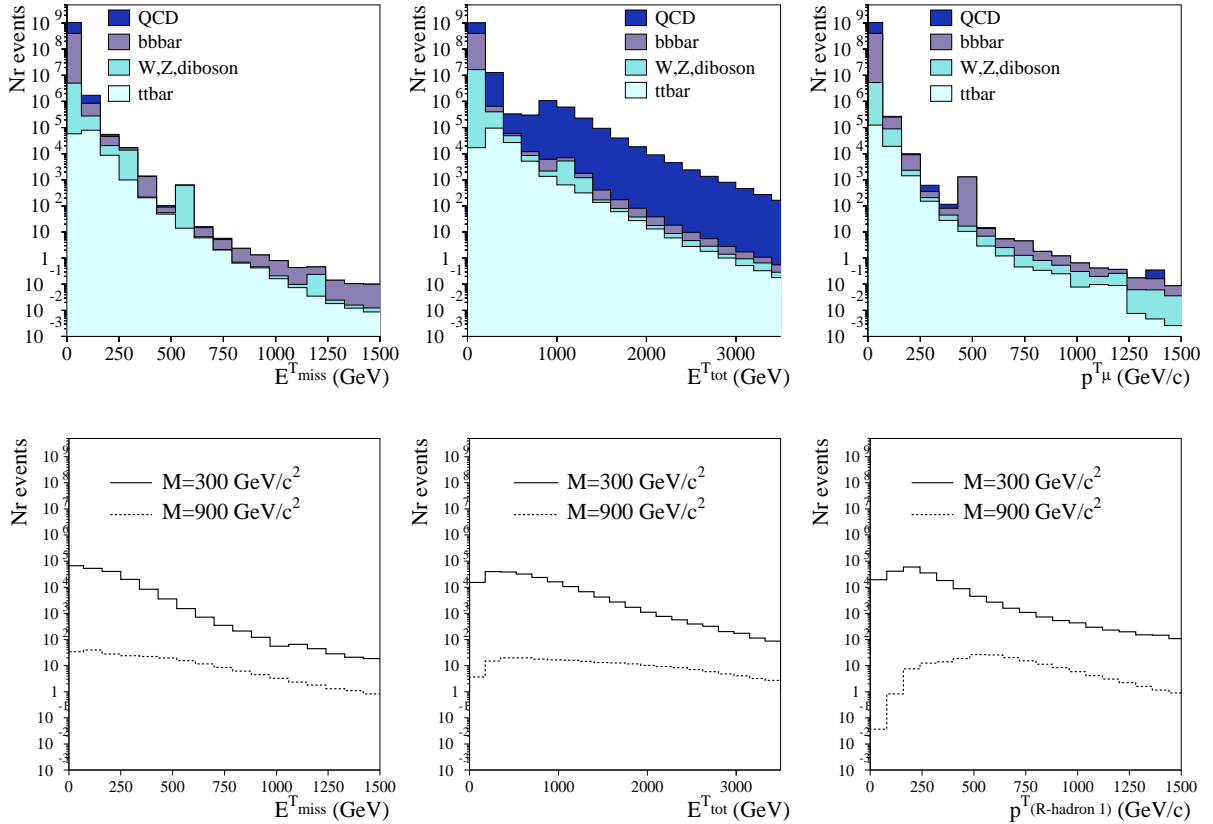


Figure 10: The missing transverse energy and the total visible energy, after high level trigger requirements for background (top) and signal (R-hadron with masses of 300 and 900  $\text{GeV}/c^2$ ). The number of events corresponds to an integrated luminosity of  $1 \text{ fb}^{-1}$ .

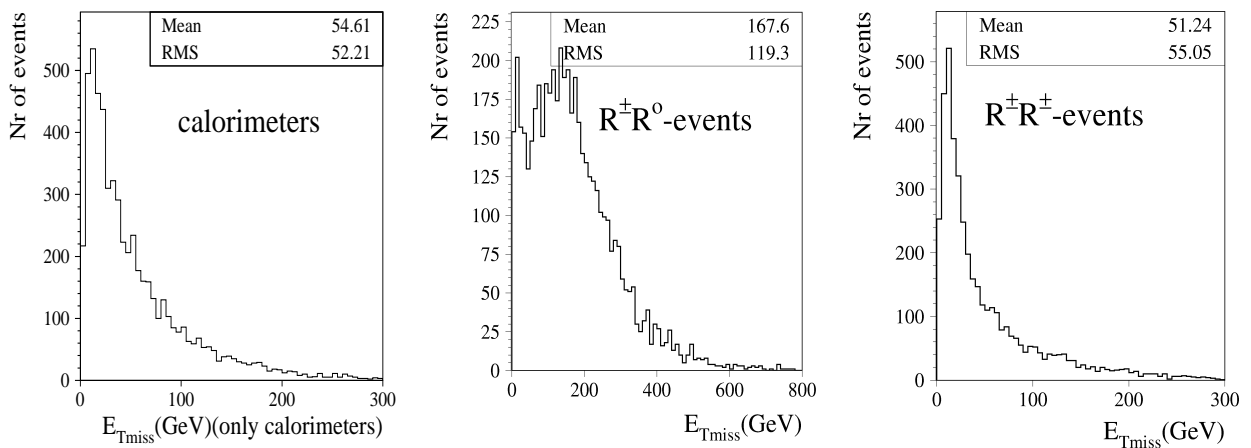


Figure 11: The missing transverse energy for R-hadrons produced via  $gg \rightarrow \tilde{g}\tilde{g}$  where  $M = 300 \text{ GeV}/c^2$  in case only calorimeter information is used (left), in case a neutral and a charged R-hadron are detected (center), and in case two charged R-hadrons (right).

Mass	Cut		
	$E_{miss}^T$ (GeV)	$E_{sum}^T$ (GeV)	$p_T^{\mu, R}$ (GeV/c)
100	> 40	> 200	> 70
300	> 100	> 250	> 135
600	> 160	> 450	> 200
900	> 250	> 600	> 280
1100	> 330	> 750	> 300
1300	> 380	> 900	> 350
1500	> 430	> 1050	> 430
1700	> 470	> 1200	> 500
1900	> 490	> 1350	> 580

Table 5: Selections for the different R-hadron masses.

the hadronization process. The extreme value of 1.0 implies that only neutral R-hadrons are produced. Due to the repeated charge flipping of the R-hadrons as they traverse the calorimeters, the R-hadron signature in the muon system is independent of the initial charge, hence, a selection based on muon-like signatures is unaffected by this parameter. For our selection using missing and visible energy and thus relying on inner detector information the significance is at most reduced by a factor 2 for events generated with  $P_{gg} = 1$ , as the momentum imbalance in the tracking system, as well as the total amount of visible energy, are smaller on average. A significance loss by a factor 2 lowers the discovery reach by about  $100 \text{ GeV}/c^2$ . Although no track is present in the inner detector, the selection is still effective, as the R-hadron can still be detected in the muon system and thereby contribute to a total energy signal. Another issue is the handling of events with neutral R-hadrons in the inner detector and charged R-hadrons in the muon system by the event reconstruction. This uncertainty has not been quantified, because a detailed knowledge of the final reconstruction software is needed. But it is not expected to be a limiting factor for discovering R-hadrons.

As shown in Table 3, R-hadrons have a non-zero probability to undergo a nuclear interaction in the muon system, and thereby possibly changing their charge. This probability can be as high as roughly 50% over the full muon system due to the presence of support structures and cryostats. As can be seen from Table 3, a large fraction of R-hadron events would actually fire the muon trigger, and the uncertainty arises thus mainly from the reconstruction of such events. In a worse-case scenario, 50% of the R-hadrons would be reconstructed badly, and simply be completely lost. In that case, the number of signal events would be reduced with a factor 2, corresponding to a decrease in the discovery reach of about  $100 \text{ GeV}/c^2$ .

Additional uncertainties related to the generation and simulation of events, such as parton distribution functions, higher order corrections and background rate uncertainties have not been studied. Furthermore, the calibration and final understanding of the detector response may influence the above results. No attempt has been made to quantify these kind of uncertainties, but given the many and very distinct signatures of R-hadrons, they are expected not to have a dramatic impact on the abilities for discovering R-hadrons over a broad mass range.

Mass (GeV/c <sup>2</sup> )	Selected background (1 fb <sup>-1</sup> )						Selected signal (1 fb <sup>-1</sup> )	S/√B (1 fb <sup>-1</sup> )	S/√B (30 fb <sup>-1</sup> )
	QCD	b̄b	t̄t	W	Z	WW/ WZ/ZZ			
100	1.3×10 <sup>4</sup>	1.1×10 <sup>3</sup>	1.2×10 <sup>4</sup>	1.7×10 <sup>4</sup>	8.2×10 <sup>2</sup>	4.5×10 <sup>2</sup>	8.7×10 <sup>6</sup>	4.1×10 <sup>4</sup>	22×10 <sup>4</sup>
300	6.2×10 <sup>2</sup>	66	7.3×10 <sup>2</sup>	2.0×10 <sup>3</sup>	37	51	8.6×10 <sup>4</sup>	1.4×10 <sup>3</sup>	7.7×10 <sup>3</sup>
600	40	6.8	85	47	65	11	1.7×10 <sup>3</sup>	1.2×10 <sup>2</sup>	6.6×10 <sup>2</sup>
900	3.1	0.6	11	13	2.0	3.2	97	17.1	93.7
1100	1.2	0.2	4.0	5.3	1.2	1.3	19	5.3	29.0
1300	0.8	0.1	1.9	2.3	0.8	0.8	3.9	1.5	8.21
1500	0.2	0.1	0.8	1.2	0.5	0.5	1.0	0.6	3.29
1700	0.1	0.0	0.5	0.7	0.4	0.2	0.25	0.18	0.99
1900	0.1	0.0	0.5	0.5	0.3	0.2	0.05	0.04	0.22

Table 6: Expected number of signal and background events for the selection presented in Table 5.

Mass	Selected signal (1 fb <sup>-1</sup> )	S/√B(1 fb <sup>-1</sup> )	S/√B(30 fb <sup>-1</sup> )
100	1.4×10 <sup>7</sup>	5.9×10 <sup>5</sup>	32×10 <sup>5</sup>
300	1.4×10 <sup>5</sup>	1.9×10 <sup>4</sup>	10×10 <sup>4</sup>
600	2.8×10 <sup>3</sup>	9.8×10 <sup>2</sup>	54×10 <sup>2</sup>
900	168	94.0	515
1100	33	42.0	230
1300	7.0	11.8	65.0
1500	1.87	4.24	23.2
1700	0.44	1.22	6.68
1900	0.08	0.24	1.31

Table 7: Ratio  $S/\sqrt{B}$  for the different R-hadron masses when replacing the cut on  $E_{miss}^T$  and  $E_{sum}^T$  by a time-of-flight cut  $\Delta\text{TOF} > 3$  n.

## 5 Possible improvements from additional R-hadron detector signatures in ATLAS

The very high selection and rejection efficiency of a time-of-flight based selection, makes it difficult to improve the selection for events with at least one well-reconstructed R-hadron in the muon detector. The remaining events have no R-hadron seen in the muon detector and a model dependent fraction may even be produced neutral at the origin. Applying an event-topology based selection is possible, but the signal significance obtained with this approach is marginal. There are however additional signatures of an R-hadron which can be utilized to select events with no R-hadron seen in the muon detector and also serve as a cross check of event with an R-hadron in the muon detector. In this section we discuss how the selection could be improved, potentially allowing R-hadrons with even higher masses to be discovered, by making use of more detailed detector information such as the TRT, the E/p ratio, and shower profiles in the calorimeters.

### 5.1 Signatures in the inner detector

For events with at least one charged R-hadron produced in the hard process, the typically slow charged R-hadron will deposit large ionization energy signals in the tracking system. Since the TRT has been designed for accurate  $dE/dx$  measurements, this subdetector has been investigated in more detail. A similar possibility exists for the ATLAS pixel detector.

#### 5.1.1 Signatures in the TRT detector

The ionization energy deposits of a slow charged particle grow approximately like  $1/\beta^2$ . Hits in the ATLAS TRT detector are registered using two discriminator levels: a low threshold level, corresponding approximately to 200 eV, and a high threshold level, corresponding to a transition radiation photon of about 5 KeV. The time of the low threshold crossing is measured with a 3.125 ns binning. With these measurements, R-hadron identification can be achieved in two (highly correlated) ways: by counting the number of straw hits exceeding the high threshold (HT) discriminator level [25] or by using the Time-over-Threshold method (ToT) [25, 28, 29].

**Counting HT hits.** To study the number of high threshold hits of R-hadrons, and to compare them with those of electrons and muons, R-hadrons of different mass ( $100 \text{ GeV}/c^2$ ,  $300 \text{ GeV}/c^2$ ,  $600 \text{ GeV}/c^2$ ), as well as muons and electrons with various transverse momenta and  $\eta$ -values have been generated, simulated and reconstructed.

In Fig. 12a the number of straws crossed by a particle is displayed as function of  $\eta$ . The number of crossed straws varies with  $\eta$ , and so does the average amount of high threshold hits. The TRT detector is therefore divided into five  $\eta$  regions, and the average amount of high threshold hits is studied as function of  $\beta\gamma$  of the particle.

For the ATLAS fast simulation framework a parameterization of this average is made with fluctuations described by a Poisson distribution. Thus, given the particle's  $\eta$  and  $\beta\gamma$  value, the number of high threshold hits can be generated by a Poisson distribution around the mean value as given by the parameterized functions.

As it can be seen from Fig. 12b, HT hits can play a role for R-hadron identification only for  $\beta\gamma \lesssim 1$ , or  $\beta \lesssim 0.7$ . On the other hand, the number of HT hits can be used to separate fast R-hadrons with  $\beta \gtrsim 0.7$ , when they are minimum ionizing, from very high  $p_T$  muons ( $p_T \gtrsim 200 \text{ GeV}/c$ ) which start to emit transition radiation photons.

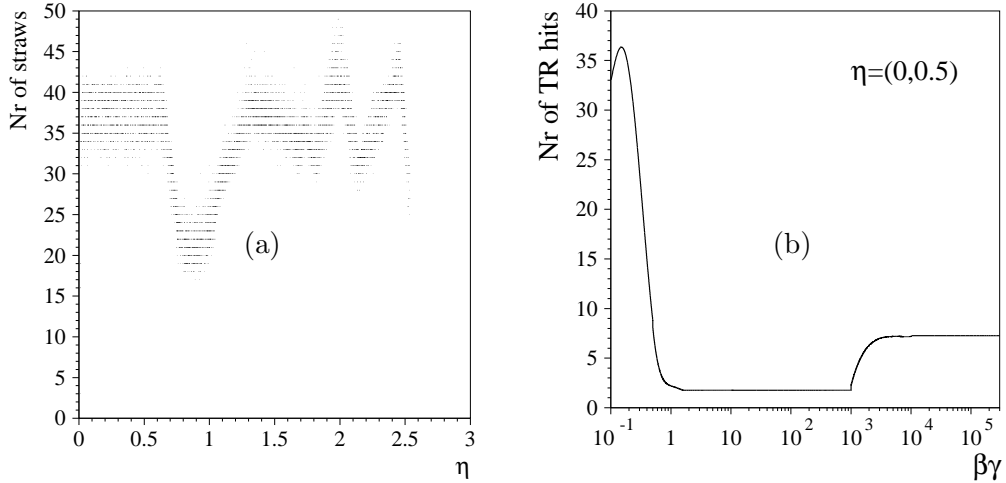


Figure 12: (a) The number of crossed straws as function of R-hadron pseudo-rapidity. (b) Average number of HT hits as function of  $\beta\gamma$  of a particle at central pseudo-rapidity.

**Time-over-Threshold.** By using the Time-over-Threshold method (ToT) [25, 28, 29], i.e. measuring time in which a signal is above the low threshold discriminator level. In general, the more energy a particle deposits, the longer the signal will remain above the threshold, and thus, by measuring the time elapsed between a signal exceeding and falling below the threshold, it is possible to extract information about the  $dE/dx$ . It is possible to identify particles by their average energy deposits in a straw per unit distance  $dE/dx$ . Rather than recording the amplitude, proportional to energy loss, the TRT electronics can measure the time of a signal being above the low threshold. This time depends on the hit distance to the anode in the straw (the closer to the anode wire the track is located the larger the ToT) and on the deposited energy (a heavily ionizing particle manifests itself by a large ToT). These can be used in two ways for the R-hadrons identification<sup>4</sup>:

- Using the traversed length to normalize the ToT in the straw. Translating the hit distance to the anode into the traversed length in the straw, and remembering that  $dE \sim x$ , we expect the ToT of a straw to be linear dependent on the traversed length  $x$ . However, Fig. 13a shows a different behaviour: the ratio increases significantly if the straw is hit very close to the anode wire. Although a fit with a straight line is possible, the increase of the ToT at small hit distances from the wire makes this method inappropriate to establish the dependence of the ToT on the  $dE/dx$ .
- To use the relation between the ToT averaged over all hit distances in a straw,  $\langle \text{ToT} \rangle$ , on the  $dE/dx$  following from the Bethe-Bloch description. In Fig. 13b the  $\langle \text{ToT} \rangle$  is displayed as function of the theoretical  $dE/dx$ . The linear dependence between the  $dE/dx$  of the particle and its  $\langle \text{ToT} \rangle$  in a straw enables us to extrapolate the  $dE/dx$  for R-hadrons in the region of the Bethe-Bloch function where  $dE/dx$  is proportional to  $1/\beta^2 \times dE/dx(\text{mip})$  and to obtain the expected  $\langle \text{ToT} \rangle$ . As is shown in Fig. 13c, the  $\langle \text{ToT} \rangle$  has a Gaussian distribution. To estimate the separation power of the ToT method between heavy hadrons

<sup>4</sup>This analysis has been done using test beam data with the TRT electronics developed in 1999. Recently, the TRT electronics was changed to provide a more stable drift time measurements independent on the signal amplitude. This makes ToT measurement less sensitive to the particle  $dE/dx$ .

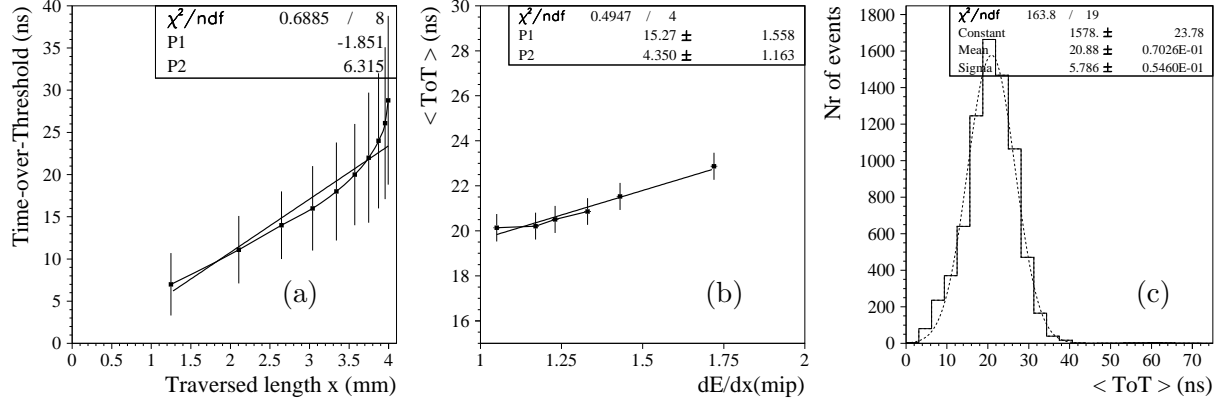


Figure 13: (a) The time-over-threshold (ToT) as function of the traversed length in the straw for a 5 GeV pion, fitted with a first degree polynomial [29]. (b) The relation between the  $dE/dx$  of a pion, and its average ToT. (c) A 1-dimensional projection of the ToT for central values (between 0.8 and 1.2 mm) of the distance of closest approach, fitted with a Gaussian.

and for example pions, a simulation experiment is done with 100000 measurements, for different  $\beta$  values, and an average ToT is generated and compared to that of ultrarelativistic pions. Results are displayed for pions and R-hadrons with momenta of 400  $\text{GeV}/c$  in Fig. 14. It is seen that for R-hadrons with velocities  $\beta = 0.55$ ,  $\beta = 0.71$  and  $\beta = 0.95$  a separation of  $5.2\sigma$ ,  $1.0\sigma$  and  $1.6\sigma$ , respectively, can be obtained.

Note that for high  $\beta$  values the R-hadron becomes less ionizing than an ultra-relativistic pion.

The number of high threshold hits and the  $\langle \text{ToT} \rangle$  in the TRT are the only estimators of  $dE/dx$  available in ATLAS. These estimators are very highly correlated, so that the separation power of the two together is only marginally larger than the separation power of the best single estimator.

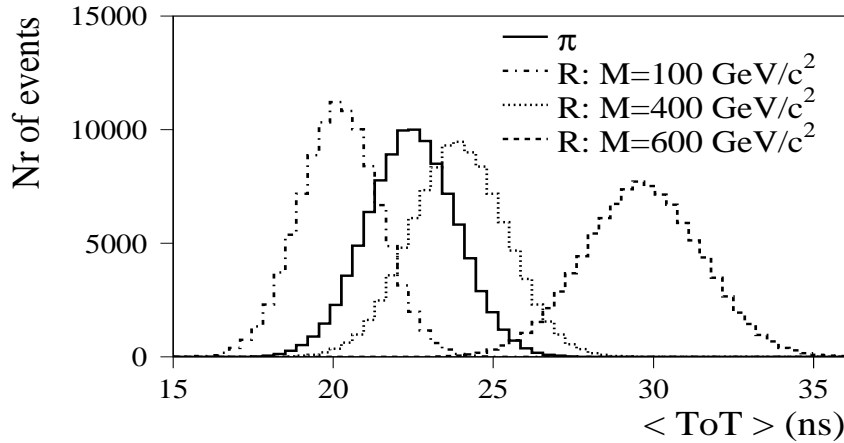


Figure 14: The average ToT for a particle hitting 33 straws (the average over all eta values) for pions of momentum 400  $\text{GeV}/c$  (solid curve) and for R-hadrons with momentum 400  $\text{GeV}/c$  and mass  $100 \text{ GeV}/c^2$  (or  $\beta = 0.95$ , dashed-dotted), mass  $400 \text{ GeV}/c^2$  (or  $\beta = 0.71$ , dotted), and mass  $600 \text{ GeV}/c^2$  (or  $\beta = 0.55$ , dashed). Note that results only depend on the velocity.

## 5.2 Matching inner detector and calorimeters

The low energy deposits from an R-hadron passing the calorimeters (Fig. 4) makes the comparison of the momentum measurement of the track with energy deposits a potential useful separation variable against pions and electrons. In Fig. 15, the ratio of the total measured

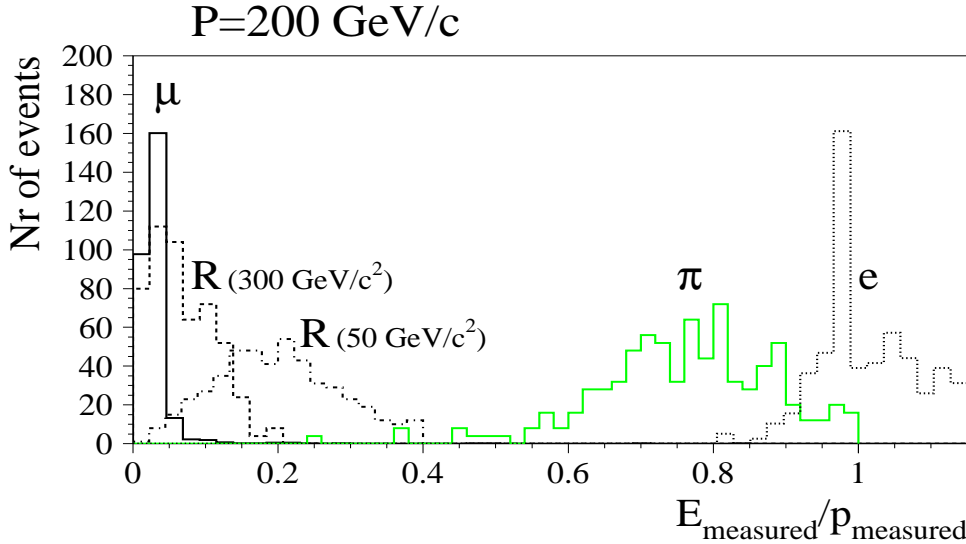


Figure 15: The ratio  $E/p$  for R-hadrons, muons, pions and electrons in the barrel region ( $\eta = 0.1$ ). Singly charged R-mesons, muons, pions and electrons are generated and reconstructed. The two extreme cases are represented by the muons (solid line) and the electrons (dotted line).

energy in the calorimeters and the momentum of the track,  $E/p$ , is displayed for R-hadrons, muons, electrons and pions in the barrel region.

## 5.3 Signatures in the calorimeters

Due to the charge flipping nature of R-hadron nuclear interactions and the model dependent production rate of neutral R-hadrons, the *only* certain signature of an R-hadron is its energy deposit in the ATLAS calorimeters.

In principle the ATLAS calorimeters can also be used to provide time-of-flight information but given the low energy deposits and the delayed arrival of slow R-Hadrons, the time determination will have a larger uncertainty. An additional uncertainty is the propagation time on the shower development for an R-hadron, which has not been available in the GEANT3 study.

### 5.3.1 Longitudinal calorimeter profile

The longitudinal energy deposit profile for fully simulated R-hadrons has been studied and compared to those of electrons and pions in the different calorimeter compartments of the ATLAS detector.

Differences are due to the fact that the typical energy loss per interaction for R-hadrons is small relative to the R-hadrons energy. Contrary to energy losses of electrons or pions, the R-hadron energy deposits remain fairly constant along the trajectory of the particle, however it

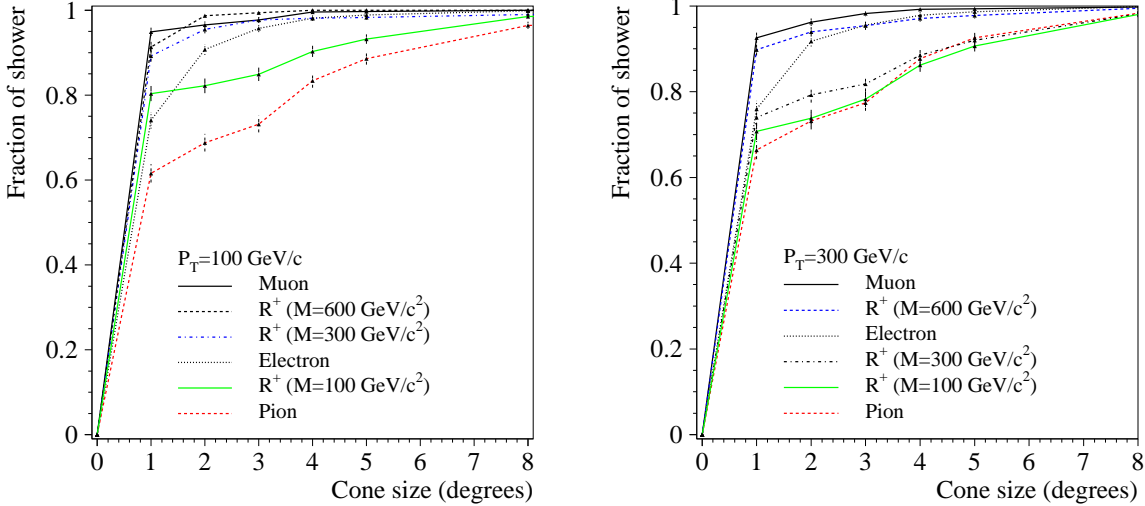


Figure 16: Lateral energy profile for muons, electrons, pions and R-hadrons of different masses with  $p_T = 100$  and  $300$   $\text{GeV}/c$ .

should be emphasized that this is only approximately true when nuclear interactions are dominating; for low  $\beta$  (e.g. when particle is significantly slowed down) the usual electromagnetic energy loss is dominating. Since R-hadrons typically are produced with high momenta relative to their mass and thus high kinetic energy, the constant energy deposit approximation generally holds, and the energy deposit is linearly proportional to the thickness of a calorimeter compartment. In this aspect R-hadron profiles are similar to those of minimum ionizing particles like muons, apart from the absolute scale of the energy deposits. For example, an R-hadron of mass  $300$   $\text{GeV}/c^2$  and momentum  $200$   $\text{GeV}/c$ , the averaged energy deposits in the tile calorimeter compartments amount to  $2.5$ ,  $6.2$  and  $3.0$   $\text{GeV}/c^2$ , for corresponding thicknesses of  $1.4$ ,  $3.9$  and  $1.8$  interaction lengths, respectively. Note, however, that although the *average* profiles for muons and R-hadrons are similar, the event-by-event variation for R-hadrons, due to charge-flipping and fluctuations in the energy loss, are considerably larger than for muons.

### 5.3.2 Lateral calorimeter profile

The lateral energy profile is investigated and compared to that of pions, muons and electrons. The width of an R-hadron shower is determined as the fractional energy measured inside a wedge as function of its opening angle. The energy is calculated as the sum of the calibrated cell energies in the ATLAS calorimeters.

The results are shown in Fig. 16 for particles generated in the central detector region, with an  $\eta$  value in between  $0$  and  $0.1$ , and an arbitrary  $\phi$  direction. Due to the nuclear interaction nature of the R-hadron shower, the shower can be quite broad, depending on the R-hadron kinetic energy. It can be seen that for R-hadrons with large kinetic energy, the shower can be as wide as that of a pion (for very high energies even broader), while slow R-hadrons exhibit showers which are as narrow as muon showers. However, the full shower shape depends highly on the amount of other particles produced in the hadronization process. Although the broadness of the shower profile could possibly be used in discriminating R-hadrons from other particles, in particular from high  $p_T$  muons, a detailed parametrization and understanding of the event-by-event fluctuations of the shower width is left for a future study.

## 6 Conclusion

In this paper we have addressed many aspects important for the detection of heavy hadronically interacting particles with exotic and complex signatures in the detector: R-hadrons. Using only a few general observables and making use of standard detector techniques with the ATLAS detector would allow the discovery of R-hadrons with a mass reach of at least  $1400 \text{ GeV}/c^2$  for an integrated luminosity of  $30 \text{ fb}^{-1}$  at low luminosity running. R-hadrons with masses as predicted by standard SUSY scenarios ( $M < 600 \text{ GeV}/c^2$ ) could already be discovered at very early stages of the running of the LHC accelerator.

A stand-alone precision muon detector with excellent time-of-flight capabilities, such as the ATLAS muon spectrometer, improves significantly the discovery reach and allows a more model-independent search. Using only the ATLAS muon spectrometer, this paper has shown that R-hadrons produced via  $gg \rightarrow \tilde{g}\tilde{g}$  with masses below  $1700 \text{ GeV}/c^2$ , can be discovered at the LHC for an integrated luminosity of  $30 \text{ fb}^{-1}$  at low luminosity running. Including R-hadrons produced via  $pp \rightarrow \tilde{q}\tilde{q} \rightarrow \tilde{g}\tilde{g}qq$ , the discovery reach of heavy gluinos, as predicted by for example split supersymmetry models, extends up to at least  $1.8 \text{ TeV}/c^2$ .

At high luminosity the acceptance in the velocity,  $\beta$ , of the R-hadrons is reduced, due to changes in the ATLAS muon trigger configuration, but as the analysis can be performed essentially on high- $p_T$  muon like signatures, only a small reduction of the discovery potential is expected.

This paper also discusses additional R-hadron detector signatures which potentially can be used to improve the discovery reach even further.

We conclude that the ATLAS detector has excellent chances of finding R-hadrons with masses as predicted by standard supersymmetry scenarios as well as those predicted by split supersymmetry models.

## 7 Acknowledgements

This work has been performed within the ATLAS Collaboration, and we thank collaboration members for helpful discussions. We have made use of the physics analysis framework and tools which are the result of collaboration-wide efforts.

The authors would like to thank Torbjörn Sjöstrand for providing gluino hadronization routines and for many useful discussions. We are also grateful to Aleandro Nisati for discussions about the ATLAS muon trigger.

## References

- [1] H. Baer, K. Cheung and J.F. Gunion, *Phys. Rev. D* **59** (1999) 075002, and references therein.
- [2] N. Arkani-Hamed and S. Dimopoulos, JHEP0506:073,2005, hep-th/0405159.
- [3] G.F. Giudice and A. Romanino, Split supersymmetry, *Nucl. Phys. B* **709** (2005) 3, hep-ph/0406088.
- [4] G.R. Farrar and P. Fayet, *Phys. Lett. B* **76** (1978) 575.
- [5] W. Kilian, T. Plehn, P. Richardson and E. Schmidt, *Eur. Phys. J. C* **39** (2005) 229, hep-ph/0408088.

- [6] J.L. Hewett, B. Lillie, M. Masip, T.G. Rizzo, JHEP0409:070,2004, hep-ph/0408248.
- [7] A. Mafi and S. Raby, *Phys. Rev.* **D 62** (2000) 035003.
- [8] S. Raby and K. Tobe, *Nucl. Phys.* **B 539** (1999) 3.
- [9] A.C. Kraan, *Interactions of heavy stable hadronizing particles*, *Eur. Phys. J.* **C 37** (2004) 91.
- [10] C. Friberg, E. Norrbin and T. Sjöstrand, *Phys. Lett.* **B 403** (1997) 329.
- [11] T. Appelquist, H. Cheng, B.A. Dobrescu, *Phys. Rev.* **D 64** (2001) 035002.
- [12] See e.g. P.H. Frampton and P.Q. Hung, Pham Quang, *Phys. Rev.* **D 58** (1998) 057704, H. Fritzsch, *JournalPhys. Lett.* **B781978611**, P. Fishbane, S. Meshkov, P. Ramond, *Phys. Lett.* **B 134** (1984) 81.
- [13] G. Ingelman, C. Wetterich, *Phys. Lett.* **B 174** (1986) 109.
- [14] The Review of Particle Physics 2002 Edition, K. Hagiwara et al., *Phys. Rev.* **D 66** (2002) 010001.
- [15] M.L. Perl *et al.*, *Int. J. Mod. Phys.* **A 16** (2001) 2137.
- [16] A. Nisati, S. Petrarca and G. Salvini, *Mod. Phys. Lett.* **A 12** (1997) 2213.
- [17] A. Nisati, ATLAS note, ATL-DAQ-98-083 (1998); G. Polesello and A. Rimoldi, ATLAS note, ATL-MUON-99-006 (1999); S. Ambrosanio, B. Mele, A. Nisati, S. Petrarca, G. Polesello, A. Rimoldi and G. Salvini, hep-ph/0012192, Atti Accad. Sci. Torino Sci. Fis. Mat. Natur. **12** (2001) 5.
- [18] A.C. Kraan, Doctoral thesis: *Interactions and detection of R-hadrons*, Copenhagen, November 2004. Available at: <http://www.nbi.dk/~ackraan>.
- [19] M. Chanowitz and S. Sharpe, *Phys. Lett.* **B 126** (1983) 225.
- [20] F. Buccella, G.R. Farrar, A. Pugliese, *Phys. Lett.* **B 153** (1985) 311.
- [21] M. Foster and C. Michael, *Phys. Rev.* **D 59** (1999) 094509.
- [22] T. Sjöstrand, private communication;  
See also <http://www.thep.lu.se/~torbjorn/Pythia.html>.
- [23] Frank Paige, private communication.
- [24] GEANT detector Description and Simulation Tool (manual), CERN, Geneva, 1993.
- [25] The ATLAS Coll., *"ATLAS: Detector and physics performance technical design report. Volume 1"*, "CERN-LHCC-99-14".
- [26] ATLAS Level-1 Trigger, Technical Design Report, CERN/LHCC/1998-14, 1998.
- [27] ATLAS High-Level Trigger, Data Acquisition and Controls, Technical Design Report, CERN/LHCC/2003-022, 2003.
- [28] ATLAS Inner Detector, Technical Design Report, CERN/LHCC/97-16, 1997.
- [29] C. Driouichi, Doctoral Thesis, Lund, 2004.